Macromolecules

Article

N-Activated 1,3-Benzoxazine Monomer as a Key Agent in Polybenzoxazine Synthesis

Danuta Trybuła, Aleksandra Marszałek-Harych, Małgorzata Gazińska, Sławomir Berski, Dawid Jędrzkiewicz, and Jolanta Ejfler*

Read Online

ACCESS | Metrics & More | Article Recommendations | Supporting Information

ABSTRACT: A novel and successful application of ring-closing reactions of aminophenols has been proposed for the formation of a new type of 1,3-benzoxazine ionic derivatives. The optimization of the reaction and detailed computational studies have been reported for the estimation of heterocyclic ring stability and its further transformation, which is crucial in the polymerization process. The molecular structure of the obtained compounds has been fully characterized by applying X-ray analysis and spectroscopic methods. The novel benzoxazines undergo an intriguing thermal reaction leading to classical benzoxazines and chloroalkanes, which is the first step of transformation before polymerization. To gain more insights into the transformation behavior of ionic benzoxazine derivatives, the Fourier transform infrared (FT-IR) spectra of gaseous products were recorded in experiments with near simultaneous FT-IR/TGA measurements. The combination of thermogravimetry with FT-IR spectroscopy enables the quantitative and qualitative characterization of thermal transformation products and clarification of the reaction mechanism. The experimental data have been verified by applying DFT(B3LYP) and DFT(M062x) theoretical studies.
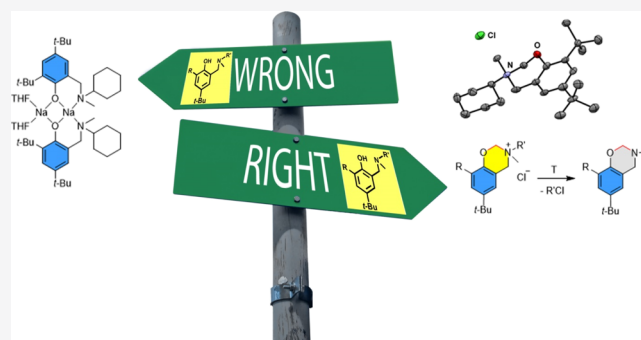
1. INTRODUCTION

Polybenzoxazines are perceived as both well-defined and still novel thermoset polymers. The appropriate tailor-made structural modification of benzoxazine monomers provides an opportunity to introduce new valuable properties into final polybenzoxazines in comparison to traditional phenolic resins.[1] The existing application of benzoxazines and polybenzoxazines in various fields is incontestable and still requires further attention. They are already widely applied in the areas of coatings, adhesives, microelectronics, and aerospace technology.[2] The advantages and features worth underlining include low water absorption,[3,4] excellent dimensional stability, nearly zero volumetric shrinkage,[5,6] thermal stability, chemical resistance,[7,8] stable low dielectric properties, self-extinguishing/flame retardance, and good electronic properties.[9−12] Additionally, it is important to note from a green chemistry point of view that the polymerization process proceeds without catalysts, byproducts, and harmful volatile formation,[13−15] and the monomers can be obtained from the renewable feedstock. In this context, biobased polybenzoxazines are a vibrant area for research.[16,17]
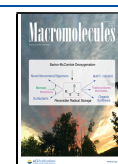
Although benzoxazine monomers possess rich molecular design flexibility, which enables the synthesis of polybenzoxazines with tailor-made properties,[18−23] some features are still being analyzed and require detailed studies in order to obtain polybenzoxazines with predictable fixed properties. On the other hand, they also have some disadvantages, such as low solubility, a high curing temperature, low fracture toughness, and a sometimes expensive fabricating process, which would require some improvements to be introduced into the monomer design on the synthesis level.

The basic strategy usually applied involves synthesizing curable polymeric benzoxazine precursors, blending the benzoxazine monomer with toughening agents, and other resins prior to the polymerization process. However, within scientific research and in industrial use, there is a growing amount of attention being paid to conducting detailed studies aimed at designing new benzoxazine monomers for the reduction of some deficiencies in order to improve their properties and add new functions. One such study presented in this paper involves the synthesis of new benzoxazine monomers and the evaluation of their heterocyclic ring stability crucial in the polymerization process. To the best of

Scheme 1. Synthetic Strategy for the Ring-Closure Reaction for 1,3-Benzoxazine Derivative Formation

our knowledge, no examples of ionic benzoxazines have been synthesized until now. While it is true that no ionic benzoxazine monomers have yet been reported, ionic polybenzoxazines have been obtained but in the post-polymerization process.[24,25] The advantages of the obtained compounds result from both the novel type of functional benzoxazine monomers and their unexpected but surprising reactivity, that is, their thermal-induced transformation to a neutral entity and chloroalkanes. The experimental results have been verified through detailed theoretical studies, which clearly demonstrate that an unexpected synthetic pathway and further transformation are possible and selective. Additionally, the new benzoxazine monomers give new insights into gaining a better understanding of the initiation stage of the ring-opening reaction of benzoxazine monomers and the new next stage of this reaction which has never been discussed in the available literature on the topic. The title compounds present a structural motif of an N-activated benzoxazine species postulated in the polymerization mechanism.

2. RESULTS AND DISCUSSION

The most widely adopted method for the synthesis of benzoxazine monomers is the classical multi-component Mannich condensation of phenols, primary amines and formaldehyde in a 1/1/2 molar ratio.[26] Until now, this was the most explored and basic method and is expanded on many different modifications to optimize the results and improve the

yields. Other synthetic routes include the ring closure of *ortho*-hydroxybenzylimine with an aldehyde,[27] the rhodium-catalyzed rearrangement reaction of functionalized benzylamines with a mixture of H_2/CO,[28] the direct reaction of ortho-lithiated phenols with N,N-bis[(benzotriazol-1-yl)methyl]amines,[29] the redox reaction of aromatic hydroxyl aldehydes and cyclic amines.[30] Both benzoxazine ring formation and modifications of the heterocyclic ring of 1,3-benzoxazines are achieved by using simple formaldehyde or more complex aldehydes. It seems that the potential of the Mannich reaction has been exhausted; however, the formation of the heterocyclic ring may proceed in a different way without using aldehyde substrates. Therefore, we studied the possibility of the ring-closing reaction of aminophenols by replacing the formaldehyde with dichloromethane as a source of the methylene bridge necessary for the formation of the 1,3-benzoxazine motif (Scheme 1).

Recently, we reported a unique method of bisphenol/bisnaphthol synthesis found as an invisible stage of an aminophenol methylation reaction. In this unexpected case, sodium complexes generated during the activation of the aminophenols played the role of crucial intermediates in the synthetic scenario.[31] These studies became the inspiration to undertake investigations of the new benzoxazine motif. Along this line, a slight change in the reaction medium and the careful analysis of synthetic nuances has provided the opportunity to

discover the ring-closing reaction of activated aminophenols, constituting a totally new approach in this area.

Designed for the needs of this study, the aminophenol $_{R,tBu}L^{R',Me}$–H was activated by an NaH in a CH_2Cl_2/THF solution. The applied solvent CH_2Cl_2 generated a methylene bridge in a ring-closure reaction leading to 1,3-benzoxazine derivative formation $[_{R,tBu}Bx^{R',Me}]Cl$ (Scheme 1). The synthetic strategy has been verified by using two types of aminophenols with a free or bulky ortho-position of the aryl core and two types of amine arms containing an alkyl chain (C12) or cyclohexyl ring (Cy). The structure of the obtained compounds $[_{R,tBu}Bx^{R/Me}]Cl$ in the solution and in the solid state were determined by using NMR spectroscopy and the X-ray crystallography method (for details of the X-ray data and NMR spectra, see Supporting Information, Figures S1–S4, Tables S1 and S2). The ^1H NMR spectrum of $[_{R,tBu}Bx^{R/Me}]Cl$ compounds revealed signals revealing the presence of tert-butyl groups, aryl protons, and a Cy or dodecyl chain. However, the most important were the signals in the range 3.38–3.59 ppm which was assigned to the presence of the methyl substituent on the nitrogen atom and the signals in the range 5.39–5.76 ppm attributed to a newly formed methylene bridge that appeared during the ring-closing reaction. The formation of the heterocyclic ring has been observed in the presence of CD_2Cl_2 in the reaction media (Figure 1, example for $[_{dtBu}Bx^{Cy,Me}]Cl$).
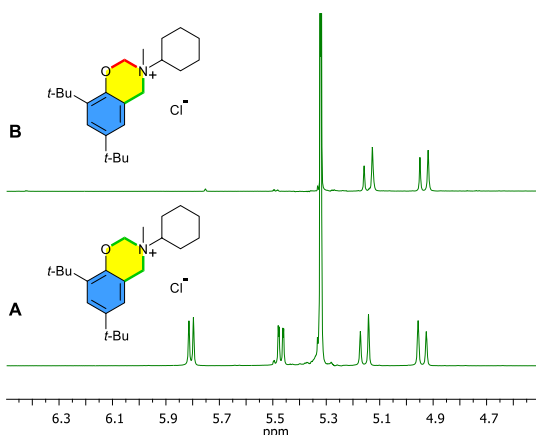
Figure 1. Fragment of ^1H NMR spectra for $[_{dtBu}Bx^{Cy,Me}]Cl$ formed in the presence of CH_2Cl_2 (A) or CD_2Cl_2 (B).

The absolute assignment of the molecular structures of two isomers for $[_{dtBu}Bx^{Cy,Me}]Cl$ was achieved by applying X-ray crystallography (Figure 2). The isomers represent a different arrangement of the methyl and cyclohexyl substituents occurring on the nitrogen atom. The crystallographic data reveal that all bond lengths and angles are in the normal ranges
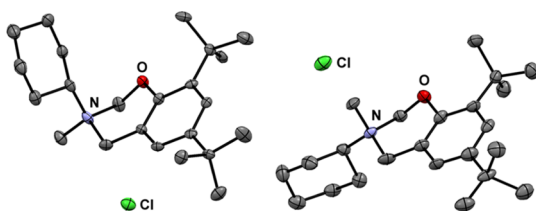
Figure 2. Molecular structures of two benzoxazine $[_{dtBu}Bx^{Cy,Me}]Cl$ isomers (isomer 1—right, isomer 2—left).

and comparable to reported neutral ones (for details of the X-ray data, see Tables S1 and S2),[14,21,32] but it should be emphasized that this is the first example of ionic 1,3-benzoxazine in the literature. The heterocyclic ring presents a preferential distorted semichair conformation, making it possible for the oxazine ring to undergo ring-opening polymerization (ROP). This structural feature is a paradigm for classical benzoxazines, but here it also indicates the ability to achieve ring opening.

Therefore, joint computational and experimental studies have been undertaken, as they may provide some mechanistic information for the better understanding of both the stability and ability to transform the benzoxazine heterocyclic ring and for the comparison of neutral and ionic species.

Both types of benzoxazines, the neutral $_{R,tBu}Bx^{Cy}$ and the $[_{dtBu}Bx^{Cy,Me}]Cl$, have been studied, and the effect of the solvent has been taken into account by means of micro solvation with four CH_2Cl_2 molecules. The calculations have been carried out using the DFT method with four electron density functionals (B3LYP,[33−36] M062x,[37] PBE0,[38] B3PW91[39] and the 6-31+G(d,p) basis set[40−43]). Exemplary structures optimized at the DFT(M062x)/6-31+G(d,p) computational level[42−44] for both $_{dtBu}Bx^{Cy}$ and $[_{dtBu}Bx^{Cy,Me}]Cl$ with four dichloromethane molecules models have been presented in Figure S11 (see Supporting Information).[45,46]

The calculated energies of the highest occupied (HOMO) and lowest unoccupied molecular orbitals (LUMO) have been presented in Figure 3 and Table S2. The HOMO−LUMO gap
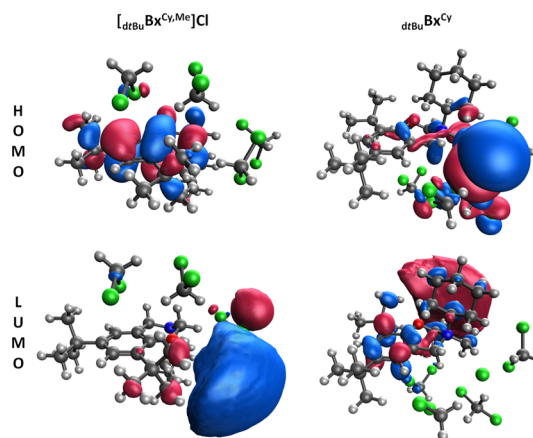

Figure 3. HOMO and LUMO. Ionic $[_{dtBu}Bx^{Cy,Me}]Cl$—left, neutral $_{dtBu}Bx^{Cy}$—right.

for the $_{R,tBu}Bx^{Cy}$ model oscillates between 3.32 (PBE0) and 7.37 eV (M062x), while for the $[_{R,tBu}Bx^{Cy,Me}]Cl$ (ionic) model—between 2.80 (PBE0) and 7.40 eV (M062x). With the exception of the M062x calculations, carried out for the molecules with substituents in the ortho-positions and solvent molecules, which indicate a slightly (0.105 eV) larger LUMO−HOMO gap for the neutral form, in all other cases the HOMO−LUMO gap for the $[_{R,tBu}Bx^{Cy,Me}]Cl$ (ionic) model is smaller than for the $_{R,tBu}Bx^{Cy}$ model. Thus, one may expect smaller thermodynamic stability for the ionic system. It is worth emphasizing that the difference in the energy gaps between both molecules is only 0.52 eV in the PBE0 calculations, while for the B3LYP, B3PW91, and M062x methods similar values are obtained in the range: 1.27−1.41

Scheme 2. Mechanism of Benzoxazine Polymerisation Leading to Phenoxy-Type Polybenzoxazine by O-Activation (Left) or N-Activation (Right)
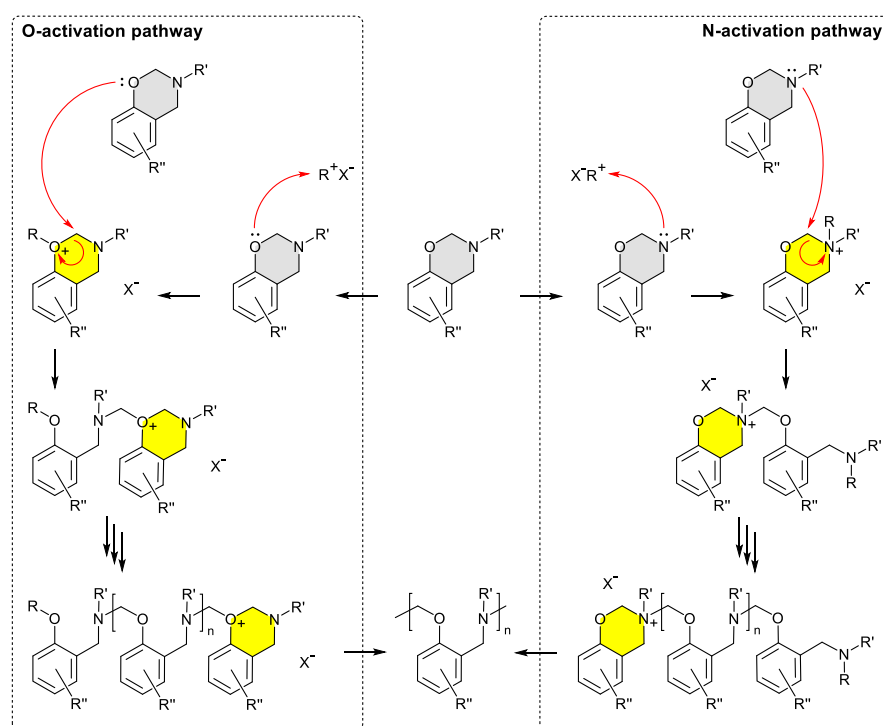
Scheme 3. Mechanism of Benzoxazine Polymerisation Leading to Phenolic-Type Polybenzoxazine by O-Activation (Left) or N-Activation (Right)
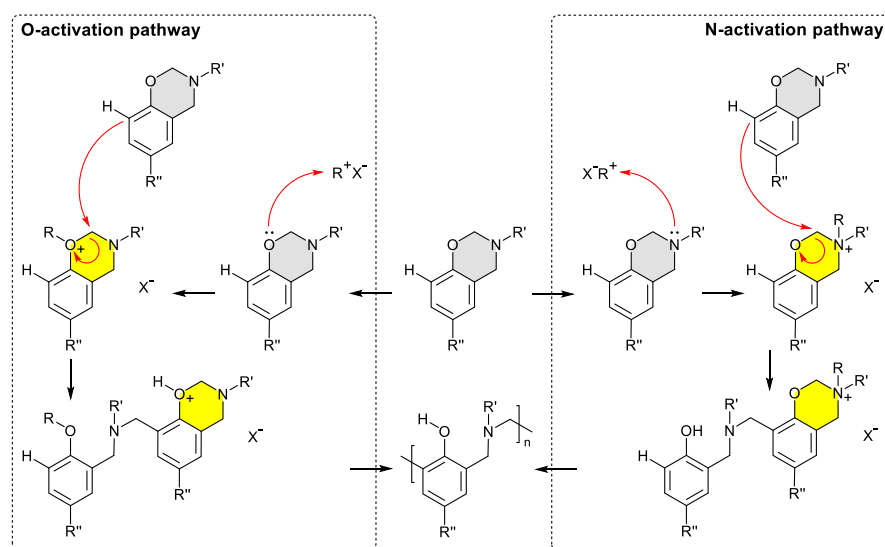
eV. The results indicated that neutral benzoxazine is more stable than the N-activated benzoxazine species $_{R,tBu}Bx^{Cy}$.

In the commonly proposed mechanism of the ROP of benzoxazine, the oxygen over nitrogen as the initiation site is preferred, and then with a cyclic tertiary oxonium ion formed by the O-activated oxazine ring. Polymerization by the O-activated species leads to a phenoxy-type polybenzoxazine structure (Scheme 2, left).

However, an alternative polymerization pathway is also possible through the N-activated oxazine ring, giving the same type of polybenzoxazine (Scheme 2, right). Although this alternative mechanism has been proposed, it has never been proven experimentally. Additionally, the substituents located on the aryl core of the benzoxazine monomer influence the type of polymer formation created, which was described in detail in our earlier studies.[14] The obstructed ortho position in the aryl core of the benzoxazine monomer selectively forms phenoxy-type polybenzoxazine. On the other hand, the benzoxazine monomers with a free ortho position possess high reactivity toward polymerization with or without catalysts and commonly form a phenolic-type polymer. Similarly, for this type of polymers, the O-activated species is favored. The obtained here benzoxazine monomers are the well-defined N-

Scheme 4. General Scheme of Three Possible Decomposition Reactions of the [$_{dtBu}$Bx^{Cy,Me}]Cl Benzoxazine
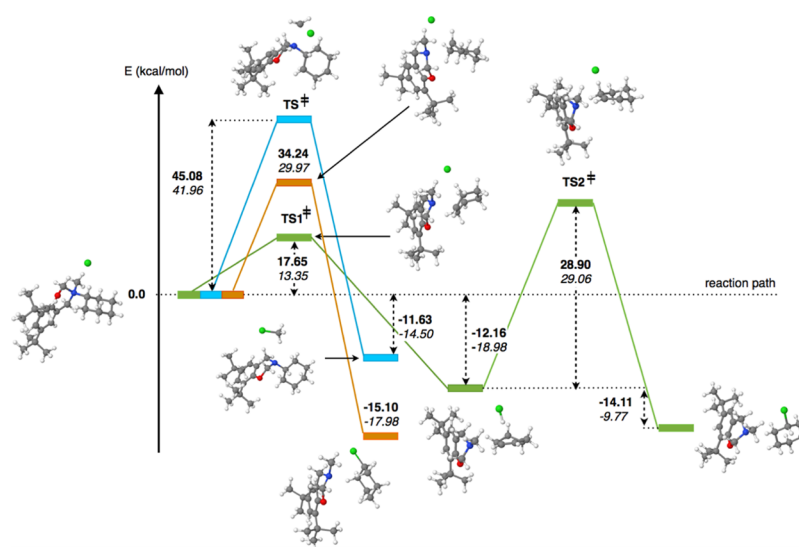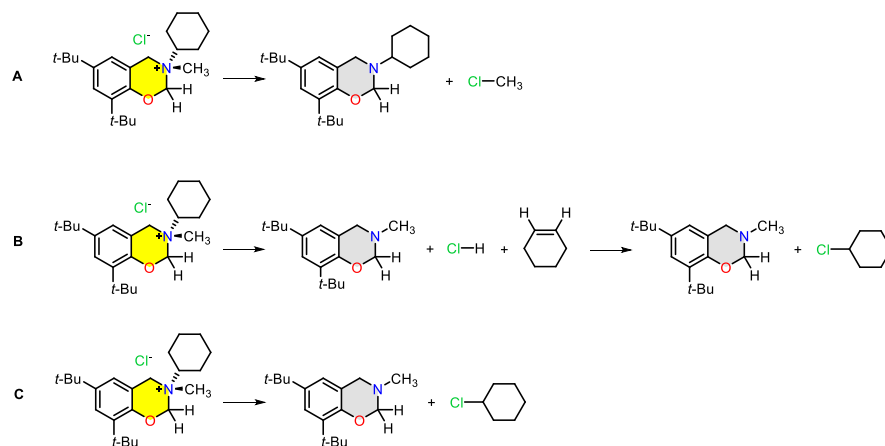
Figure 4. Schematic energy profiles of three decomposition reactions of the [$_{dtBu}$Bx^{Cy,Me}]Cl benzoxazine. (A) Blue line, (B) green line, and (C) orange line. The numerical values correspond to the activation energies (E_a) calculated from the side of the reagents and the reaction energies. In cursive the values corrected by ΔZPVE.

activated form synthesized in two versions of the aryl core (Scheme 3).

The evaluation of the potential application of benzoxazine monomers required an analysis of their thermal behavior, since the most important factor is the stability of the monomer's temperature just before polymerization. In order to gain more insight into the process of the transformation of the obtained ionic benzoxazines [$_{dtBu}$Bx^{Cy,Me}]Cl, three potential reactions have been investigated, one giving chloromethane (Scheme 4A) as a by-product, two other—chlorocyclohexane (Scheme 4B,C). The studies have been performed at the DFT computational level,[42−44] using the B3LYP electron density functional[33−36] and 6-31+G(d,p) basis set.[41−43] The reaction path has been simulated in vacuum at 0 K using the intrinsic reaction coordinate (IRC) procedure[47,48] (see computational details, Supporting Information).[49]

The reaction starts with the formation of the Cl$^-$···$_{dtBu}$Bx^{Cy,Me} molecular complex, and the interaction energy (E_{int}) equals −87.49 kcal/mol. Removing the basis set superposition error, using the counterpoise technique (CP), yields the value of −87.19 kcal/mol (E_{int}^{CP}).

The first stage of the decomposition reaction giving chloromethane (Scheme 4A, marked as light blue in Figure 4) has been carried out through the single transition state (TS), located at 45.08 kcal/mol (activation energy, E_a), which is above the energy level of the Cl$^-$···$_{dtBu}$Bx^{Cy,Me}. The lower value of E_a equaling 41.96 kcal/mol is obtained when the value of the zero-point vibrational energy difference (ΔZPVE) is taken into account. The analysis of the geometrical structure of TS shows that the N−CH$_3$ bond (2.295 Å) is already broken and the H$_3$C−Cl bond (2.637 Å) has not yet been formed. Thus, the TS contains the [CH$_3$]$^{0.32+}$ moiety interacting with the [$_{dtBu}$Bx^{Cy}]$^{0.28+}$ fragment and the Cl$^{0.60−}$ anion. Such an interpretation is supported by the topological analysis of the electron localization function (ELF),[50−52] which shows the lack of the bonding basin V(C,N) and the lack of any bonding basin formed by the Cl atom (separated Cl atom). On the other hand, one may observe a lone pair in the vicinity of the N atom, V(N), with 1.74 e, which is the remainder of the heteropolar N−C(CH$_3$) bond. The N−C bond, formed by the C atom from the cyclohexyl group, is described by the bonding basin V(C,N) with 1.84 e, thus, it is a single bond depleted with electron density.

Atomic rearrangement after TS leads to a molecular complex being formed between the chloromethane and the benzoxazine molecules (H$_3$CCl···$_{dtBu}$Bx^{Cy}). Both molecules interact through noncovalent interactions with E_{int} of −1.16 kcal/mol and E_{int}^{CP} of −0.85 kcal/mol. The total reaction is exothermic with reaction energies of −11.63 and −14.50 kcal/mol, when the ΔZPVE value is taken into account.

A second reaction that leads to the formation of the $_{dtBu}$Bx^{Me} and chlorocyclohexane molecules has been carried out through two TSs, TS1 and TS2 (Scheme 4B, marked as green in Figure 4). In the first stage of the studied reaction scheme, the HCl and cyclohexene molecules are formed and the next "portion" of HCl reacts with the cyclohexene ring leading to chlorocyclohexane molecule formation (Scheme 4B).

The first TS, TS1, is located at 17.65 kcal/mol, which is above the energy level of the Cl$^-$···$_{dtBu}$Bx^{Cy,Me} system. When the ΔZPVE is added, the value of E_a is decreased to 13.35 kcal/mol. It is worth noting that this activation energy is much smaller that the energy needed for the breaking of the N−CH$_3$ bond (45.08 and 41.96 kcal/mol).

In TS1, the N−C bond (2.351 Å) is already broken and the H−C bond (1.164 Å) is essentially elongated when this bond length is compared with that obtained for the H−C bonds (1.09 Å) not involved in any interactions. Thus, a partial transfer of the H atom toward the Cl atom is observed. The topological analysis of ELF shows that the basin population for the elongated H−C bond is 1.84 e. This population is noticeably smaller than the populations in the range 2.00−2.10 e computed for the unperturbed H−C bonds. In the region of the N−C bond, only the lone electron pair $V(N)$ is observed with a basin population of 1.99 e. Thus, the N−C bond in TS1 has been broken and the $V(N)$ basin is the remainder of the N−C bond. No bonding basin has been observed that is associated with the Cl atom, which stays unbound in TS1. The topological charge of Cl$^{\delta-}$ is −0.72 e. The charge of the H atom approaching the Cl atom is +0.23 e.

After TS1, the rearrangement of the atoms leads to a post-reaction compound, which consists of the HCl molecule interacting with the benzoxazine, $_{dtBu}$Bx^{Me}, and cyclohexene molecules. The optimized length of the C=C bond in cyclohexene is 1.345 Å. The topological analysis of ELF shows two bonding basins $V_{i=1,2}(C,C)$ in the region of the C=C bond, and such a topology of ELF supports the double type of carbon−carbon bonding. The total value of the $V_{i=1,2}(C,C)$ basin population amounts to 3.46 e, which is much larger than 2 e expected for the single C−C bond (2 e). The HCl···$_{dtBu}$Bx^{Me}···cyclohexene complex is weakly stabilized by noncovalent forces with an interaction energy of −5.87 kcal/mol (E_{int}^{CP} = −4.46 kcal/mol). The main stabilizing interaction comes from the C−H···N hydrogen bond. The reaction is exothermic with a reaction energy of −12.16 or −18.98 kcal/mol (+ΔZPVE).

The second TS, TS2, determines the energetics of the second reaction stage, which leads to the formation of the chlorocyclohexane and benzoxazine $_{dtBu}$Bx^{Me} molecules. The reaction proceeds by the addition of the HCl to the double C=C bond in the cyclohexene ring (see Scheme 4B). The activation energy from the side of the reagents (the HCl···$_{dtBu}$Bx^{Me}···C$_6$H$_{10}$ molecular complex) is 28.90 or 29.06 kcal/mol when the correction for ΔZPVE is included.

The analysis of the chemical bonds in TS2, performed by means of the topological analysis of ELF, shows that the [C$_6$H$_{11}$]$^{\delta+}$ molecule, the Cl$^{\delta-}$ anion, and the $_{dtBu}$Bx^{Me} molecule

form a system stabilized by noncovalent interactions. The hydrogen−chlorine bond is broken and the H atom is partially transferred to one of the sp^2 hybridized C atoms in the C$_6$H$_{10}$ molecule. Such an interpretation is supported by the population of the $V(H,C)$ basin of 1.71 e, which is much smaller than 2.00−2.11 e computed for the unperturbed H−C bonds. The Cl atom is localized at 2.892 Å from the second sp^2 hybridized C atom and chemical bonding is observed between those atoms. The topological analysis of ELF does not show any bonding basin associated with the Cl atom. The topological charge of Cl is −0.72 e. In the region of the C= C bond (cyclohexene ring), only one $V(C,C)$ basin is observed instead of two $V_{i=1,2}(C,C)$ basins, which have been localized for the C$_6$H$_{10}$ molecule in the HCl···$_{dtBu}$Bx^{Me}···C$_6$H$_{10}$ complex. Such a topological change is associated with the elongation of the C=C bond, which is partially transformed from a double to a single bond. The population of $V(C,C)$ of 2.25 e is close to a formal value of 2 e expected for the C−C bond.

After TS2, the reacting atoms rearrange to form the post-reaction system, which consists of chlorocyclohexane and $_{dtBu}$Bx^{Me} molecules. The molecules interact mainly through the C−H···N hydrogen bond with an interaction energy of −2.27 kcal/mol (E_{int}^{CP} = −1.65 kcal/mol).

The formation of the chlorocyclohexane is an exothermic process with respect to the energy of the HCl···$_{dtBu}$Bx^{Me}···C$_6$H$_{10}$ molecular complex (see Figure 4) with a reaction energy of −14.11 kcal/mol (−9.77 kcal/mol, including ΔZPVE). It seems more probable that such a process, investigated in the chosen physical conditions, will occur than the decomposition, which leads to the formation of the CH$_3$Cl molecule.

The third possibility (Scheme 4C, marked as orange in Figure 4) assumes the breaking of the C−C bond between the cyclohexyl group and the $_{dtBu}$Bx^{Me} fragment. Next, the chlorine atom forms the covalent C−Cl bond with the cyclohexyl group yielding the chlorocyclohexane molecule. The observed mechanism is similar to the reaction, which yields the H$_3$CCl···$_{dtBu}$Bx^{Cy} complex. The product of the reaction is the molecular complex formed between the chlorocyclohexane and the benzoxazine molecules (C$_6$H$_{11}$Cl···$_{dtBu}$Bx^{Me}). The reaction has been carried out through the single TS, located at 34.24 (E_a) and 29.97 kcal/mol (including ΔZPVE) above the energy level of the Cl$^-$···$_{dtBu}$Bx^{Cy,Me} complex. The total reaction is exothermic with the reaction energies of −11.63 and −14.50 kcal/mol (including ΔZPVE).

It is worth noting that the activation energy needed to break the C−C bond with the cyclohexyl group (29.97 kcal/mol) is smaller than the energy needed to detach the methyl group (41.96 kcal/mol). Thus, the route leading to the formation of the benzoxazine and C$_6$H$_{11}$Cl molecules seems to be more probable than the formation of the H$_3$CCl molecule. On the other hand, the activation energy for the detachement of the cyclohexyl group in a one stage process is higher than the values of E_a calculated for a two stage process proceeding through the addition of HCl to the C=C bond in the cyclohexene ring.

In order to investigate the effect of the solvent (dichloromethane) on the energetics of studied reactions the micro-solvation with single CH$_2$Cl$_2$ molecule has been considered. For the reaction yielding the $_{dtBu}$Bx^{Cy} and H$_3$CCl molecules, the value of the activation energy has been increased by 0.45 kcal/mol and the reaction energy has been increased by 0.93 kcal/mol. Thus, the influence of the solvent on the energetics

of the reaction is negligible. Similarly, a small effect has been found for the reaction yielding the $_{dt\text{Bu}}\text{Bx}^{\text{Me}}$ and $C_6H_{11}Cl$ molecules. The value of E_a has been increased by 1.18 kcal/mol and the reaction energy increased by 2.16 kcal/mol.

In the next step of our investigations, the verification of the theoretical results has been achieved through experimental studies. The thermal transformation behavior of 1,3-benzoxazine ionic derivatives has been studied by means of a combination of thermogravimetric analysis (TGA) and gas-phase Fourier transform infrared (FT-IR) spectroscopy.

The TGA and the first derivative TGA (dTGA) curves of 1,3-benzoxazine ionic derivatives are presented in Figure 5. Based on traces of each presented TGA curve, the thermal degradation process can be divided into a few partially overlapping stages.
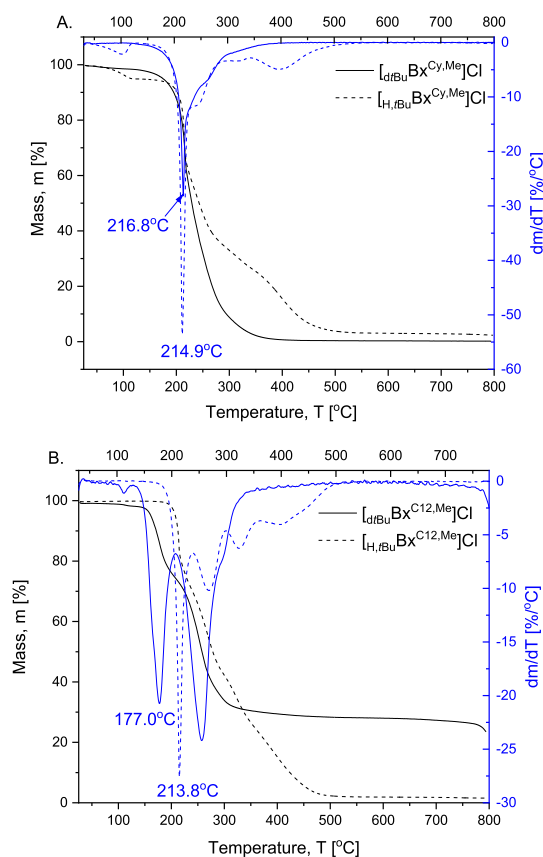
Figure 5. TGA and the first derivative TGA curves of $[_{\text{H},t\text{Bu}}\text{Bx}^{\text{Cy,Me}}]$Cl, $[_{dt\text{Bu}}\text{Bx}^{\text{Cy,Me}}]$Cl (A) and $[_{\text{H},t\text{Bu}}\text{Bx}^{\text{C12,Me}}]$Cl, and $[_{dt\text{Bu}}\text{Bx}^{\text{C12,Me}}]$Cl (B).

The common future of the dTGA curves is a distinct sharp peak with a maximum at 215 and 217 °C for the benzoxazine derivatives $[_{\text{H},t\text{Bu}}\text{Bx}^{\text{Cy,Me}}]$Cl and $[_{dt\text{Bu}}\text{Bx}^{\text{Cy,Me}}]$Cl, respectively, and at 214 °C for $[_{\text{H},t\text{Bu}}\text{Bx}^{\text{C12,Me}}]$Cl. The high temperature limit of the first degradation/transformation stage is presented in Table S3 (see Supporting Information) and corresponding mass loss occurring at this stage of degradation is in the range of 25 wt % for $[_{dt\text{Bu}}\text{Bx}^{\text{C12,Me}}]$Cl and 65 wt % for $[_{dt\text{Bu}}\text{Bx}^{\text{Cy,Me}}]$Cl (Table 1).

The degradation or more precisely transformation process of these three derivatives at higher temperatures is similar, three additional degradation stages are visible as weak overlapping peaks. The positions of the respective peaks differ depending on the structure of the benzoxazine derivatives.

Table 1. Thermal Stability of Ionic Benzoxazines

benzoxazine	mass loss at the first degradation stage [%]	$T_{-5\%}$ [°C]
$[_{\text{H},t\text{Bu}}\text{Bx}^{\text{Cy,Me}}]$Cl	43.1	115
$[_{dt\text{Bu}}\text{Bx}^{\text{Cy,Me}}]$Cl	65.5	174
$[_{\text{H},t\text{Bu}}\text{Bx}^{\text{C12,Me}}]$Cl	29.4	207
$[_{dt\text{Bu}}\text{Bx}^{\text{C12,Me}}]$Cl	25.3	161

The course of the dTGA curve of the benzoxazine derivative with an alkyl chain as the amine arm and a *tert*-butyl substituent in the ortho-position of phenol $[_{dt\text{Bu}}\text{Bx}^{\text{C12,Me}}]$Cl is different: the first stage of degradation occurs with the highest rate at the lowest temperature (177 °C). The thermal stability of this benzoxazine derivative set as the temperature corresponding to 5 wt % mass loss ($T_{-5\%}$) is lower with respect to the benzoxazine with a free ortho-position. Other differences refer to only two distinct degradation steps and the 24 wt % of residue at 800 °C.

The exemplary 3D FT-IR spectra of the gaseous decomposition products of $[_{\text{H},t\text{Bu}}\text{Bx}^{\text{Cy,Me}}]$Cl and the Gram−Schmidt curves of the benzoxazines measured near simultaneously with the TGA signal are presented in Figure 6. The Gram−Schmidt curve represents the absorbance intensity of the total gases emitted at a particular temperature; thus, the mass losses observed in the TGA are accompanied by an increase in the Gram−Schmidt curve. On the Gram−Schmidt curve of the benzoxazines, a few maxima can be distinguished. Compared with the first derivative of the TGA, there is a delay in the Gram−Schmidt maxima positions because of the transport of degradation gases through a transfer line. The combination of thermogravimetry with FT-IR spectroscopy enables the quantitative and qualitative characterization of the thermal degradation/transformation products and clarification of the reaction mechanism.

Figure 7 presents the FT-IR spectra of the gaseous degradation products of benzoxazine derivatives recorded at two temperatures selected from the temperature range corresponding to the first maximum of the Gram−Schmidt curves. The common features of FT-IR spectra presented in Figure 7 are the absorption bands characteristic for gaseous and liquid water visible at 3500−3950 and 3400−3500 cm^{-1}, respectively, and absorption bands in the range of 2250−2400, 670, and 2050−2230 cm^{-1} from carbon dioxide and carbon monoxide, respectively. The analysis of the spectra of $[_{\text{H},t\text{Bu}}\text{Bx}^{\text{C12,Me}}]$Cl acquired at a lower temperature indicates a mixture of methyl chloride and chlorododecane. The most important absorption band of stretching vibrations of the C−Cl bond, specific for alkyl chlorides, is present at 747 cm^{-1}.[53]

The presence of chlorododecane is identified by characteristic absorption bands at 2967, 2934, 2865, and 1459 cm^{-1}. The bands at 2967 and 2934 cm^{-1} correspond to the asymmetric stretching vibrations (ν_{as}) of C−H bonds of the methyl and methylene groups, respectively, whereas the band at 2865 cm^{-1} corresponds to the symmetric stretching vibrations (ν_s) of C−H bonds of methylene groups overlapping with ν_s of methyl groups.[53]

The absorption bands of the asymmetric scissoring vibrations (δ_{as}) of the C−H bonds of −CH$_3$ and the symmetric scissoring vibrations (δ_s) of the −CH$_2$− groups overlap at the range of 1476−1430 cm^{-1}. A characteristic absorption band of the symmetric scissoring vibration of the −CH$_3$ group is visible at 1373 cm^{-1}. Other bands at 2980 cm^{-1}

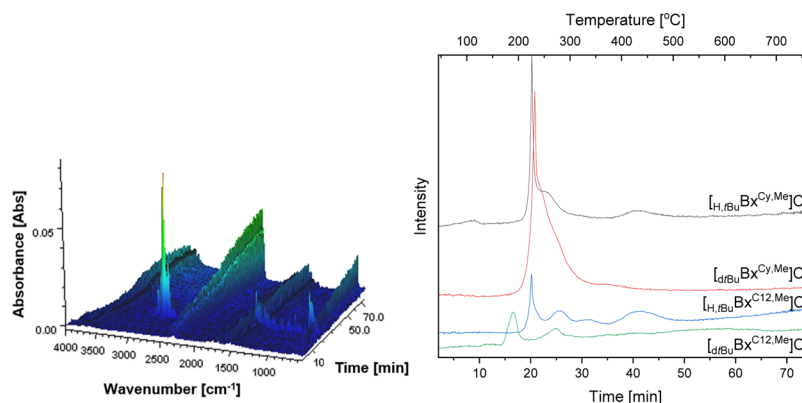**Figure 6.** Time-dependent 3D FT-IR spectra of the thermal degradation of $[_{H,tBu}Bx^{Cy,Me}]Cl$ (left) and Gram−Schmidt curves of ionic benzoxazines (right).

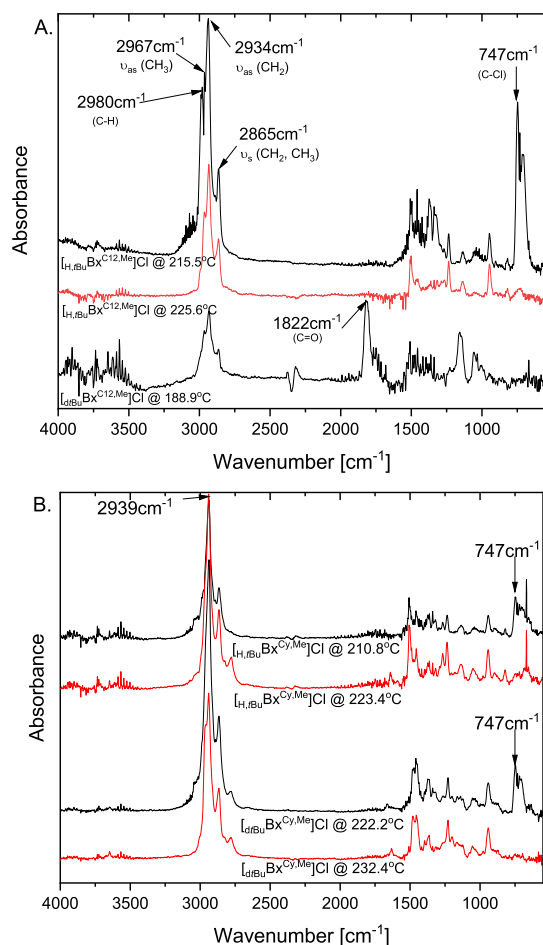**Figure 7.** FT-IR gas phase spectra of characteristic degradation products of ionic benzoxazines $[_{H,tBu}Bx^{C12,Me}]Cl$, $[_{dtBu}Bx^{C12,Me}]Cl$ (A), and $[_{H,tBu}Bx^{Cy,Me}]Cl$, $[_{dtBu}Bx^{Cy,Me}]Cl$ (B) recorded at two temperatures from the range of the first degradation stage.

(C−H stretching), 1373, and 1338 cm^{-1} attribute to methyl chloride.

The absorption band of rocking vibrations, visible typically for more than five connected −CH$_2$− groups, is present at 723 cm^{-1}. Moreover, the absorption bands of C−C skeletal vibrations at the range of 1300−800 cm^{-1} are unique for chlorododecane.[53] The recorded FT-IR spectra compared with FT-IR vapor phase spectra of chlorododecane and methyl

chloride from the infrared database of National Institute of Standards and Technology[54] are included in Supporting Information (Figure S12A).

The spectra of $[_{H,tBu}Bx^{C12,Me}]Cl$ measured at a higher temperature lack absorption bands characteristic of methyl chloride indicating that the main degradation product is chlorododecane (Figure 8). At the range of the unique group
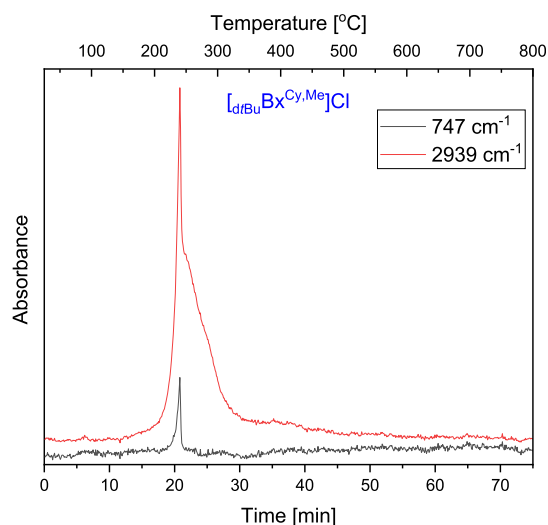

Figure 8. FT-IR profiles of wavenumbers 2939 and 747 cm^{-1} recorded during the degradation of benzoxazine $[_{dtBu}Bx^{Cy,Me}]Cl$.

frequency of the C−Cl bond stretching at 800−700 cm^{-1} remains the band with maximum at 725 cm^{-1} and weak intensity as typical for chlorododecane. The changes are also in the range 3020−2800 cm^{-1}, there is no band from methyl chloride at 2980 cm^{-1}.

The infrared spectra recorded for $[_{H,tBu}Bx^{Cy,Me}]Cl$ and $[_{dtBu}Bx^{Cy,Me}]Cl$ correspond to chlorocyclohexane as evidenced by the characteristic absorption bands at 2935, 2868, 1458, 1374, 1339, and 747 cm^{-1}.[54]

The thermal transformation of benzoxazine $[_{H,tBu}Bx^{Cy,Me}]Cl$ and $[_{dtBu}Bx^{Cy,Me}]Cl$ proceeds in an analogous manner, with the release of methyl chloride and chlorocyclohexane. The FT-IR spectra recorded at a lower temperature allow identification of methyl chloride and chlorocyclohexane, whereas the spectrum acquired at higher temperatures does not have the band characteristic of methyl chloride; the presence of chlorocyclo-

Table 2. Thermal Properties of the Benzoxazine Derivatives Estimated from the First Heating DSC Curves

benzoxazine	T_{exo}^{onset} [°C][a]	T_{exo}^{peak} [°C]	T_{exo}^{endset} [°C]	ΔH_{exo} [J/g]	mass loss up to T_{exo}^{onset} [%]	mass loss at the range of exothermic effect [%]	width of exothermic effect [°C]
$[_{H,tBu}Bx^{Cy,Me}]Cl$	219	221	227	−94.3	35.4	6.0	8
$[_{dtBu}Bx^{Cy,Me}]Cl$	215	220	244	−52.8	29.8	41.5	29
$[_{H,tBu}Bx^{C12,Me}]Cl$	212	226	252	−62.1	9.3	25.7	40

[a]Lower limit of the temperature range of exothermic peak (T_{exo}^{onset}) is estimated as the onset because of overlapping of endo- and exothermic effects.

hexane is evidenced by characteristic absorption bands at 2939, 2868, 1460, 820, and 738 cm^{-1} (see Supporting Information, Figure S12B).[54]

The rapid disappearance of methyl chloride and the evolution of chlorododecane and chlorocyclohexane as a main degradation product of the first transformation stage in the case of benzoxazine $[_{H,tBu}Bx^{C12,Me}]Cl$, $[_{H,tBu}Bx^{Cy,Me}]Cl$, and $[_{dtBu}Bx^{Cy,Me}]Cl$, respectively, is confirmed by the intensity profiles of wavenumbers 747, 2934, and 2939 cm^{-1} (Figures 8 and S13 in Supporting Information). The profile of wavenumber 747 cm^{-1} represents emission of methyl chloride, whereas wavenumbers 2934 and 2939 cm^{-1} were chosen as a characteristic for chlorododecane and chlorocyclohexane, respectively.

In the case of benzoxazine $[_{dtBu}Bx^{C12,Me}]Cl$ degradation, the mechanism is different than the one presented above. The first stage of the weight loss of $[_{dtBu}Bx^{C12,Me}]Cl$ occurs at a lower temperature as compared to other presented benzoxazines. Mass loss occurs with the highest rate at 177 °C (Figure 5). On the FT-IR spectrum of the evolved gases acquired at a temperature corresponding to the first maximum on the Gram−Schmidt curve, no characteristic absorption bands of the predicted product can be precisely distinguished (Figure 7A). The presence of other bands indicates that the evolved gases are a mixture of volatile products and the decomposition is more complex. We can hypothesize that thermal decomposition proceeds through the formation of a mixture of chloroalkanes and subsequent or sudden fragmentation of the benzoxazine ring. Such a degradation mechanism has not yet been described and requires further research on a broader group of compounds.

In the spectra of evolved gases, as shown in Figure 7, characteristic absorption bands of oxazine moieties observed at 1235 and 1228 cm^{-1} (C−O−C asymmetric stretching mode) and 943 cm^{-1} (oxazine−related bands)[55] are present and indicate on possible benzoxazine derivatives $[_{H,tBu}Bx^{C12,Me}]Cl$, $[_{H,tBu}Bx^{Cy,Me}]Cl$, and $[_{dtBu}Bx^{Cy,Me}]Cl$ evaporation at the beginning of mass loss. For comparison, ATR-FTIR spectra of benzoxazine derivatives are presented, as shown in Figure S14 in Supporting Information. This findings agree with differential scanning calorimetry (DSC) results. The presence of the large endothermic effect prior to the exothermic peak of ROP and high mass loss taking place during heating up to the onset of the ROP exotherm (Table 2) confirms some benzoxazine derivative evaporation. Partial evaporation of monomers does not disturb the elimination of chlorocyclohexane and chlorododecane during the first stage of mass loss. Evaporation of oxazine derivatives prior to polymerization was observed and described in the case of many naphthoxazine derivatives.[56,57] The absence of the characteristic absorption oxazine bands in the case of $[_{dtBu}Bx^{C12,Me}]Cl$ suggests degradation of this benzoxazine with ring opening and explains the lack of an exothermic effect on the DSC curve.

Detailed analysis of the polymerization mechanism of cationic benzoxazine derivatives $[_{H,tBu}Bx^{C12,Me}]Cl$, $[_{H,tBu}Bx^{Cy,Me}]Cl$, and $[_{dtBu}Bx^{Cy,Me}]Cl$ is planned to be described separately, and an investigation along this line is currently underway. The present study is concentrated on the explanation of the initial structural changes in benzoxazine structures occurring during heating and preceding polymerization.

The polymerization ability of the benzoxazine derivatives was verified through differential scanning calorimetry. The polymerization of benzoxazine can be confirmed by the presence of the exothermic effect at a temperature range of 200−250 °C.[1,58] The DSC curves of ionic benzoxazine derivatives are presented in Figure 9 and the estimated thermal parameters are collected in Table 2. On the DSC thermograms of $[_{H,tBu}Bx^{Cy,Me}]Cl$, $[_{dtBu}Bx^{Cy,Me}]Cl$, and
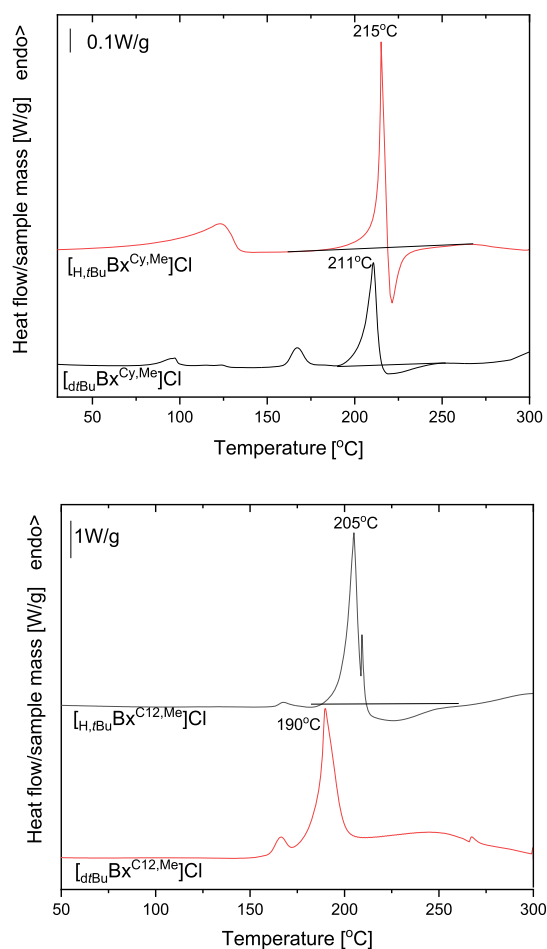
Figure 9. First heating DSC curves of benzoxazine derivatives $[_{H,tBu}Bx^{Cy,Me}]Cl$, $[_{dtBu}Bx^{Cy,Me}]Cl$ (top), and $[_{H,tBu}Bx^{C12,Me}]Cl$, $[_{dtBu}Bx^{C12,Me}]Cl$ (bottom).

$[_{H,tBu}Bx^{C12,Me}]Cl$, the exothermic effect is visible with the peak maximum (T_{exo}^{peak}) located between 210 and 226 °C. An endothermic effect overlaps at the beginning of the exothermic peak. The temperature range of this endothermic event indicates the emission of cyclohexyl chloride occurring during the first transformation stage. The endothermic peak temperatures amount to 215 °C for $[_{H,tBu}Bx^{Cy,Me}]Cl$ and 211 °C for $[_{dtBu}Bx^{Cy,Me}]Cl$ and agree with the peak temperature on the dTGA curves of the respective benzoxazine derivatives. The exothermic effect corresponds to the ROP of the benzoxazine.[58,59] In the case of typical benzoxazine precursors, ROP is accompanied by excessive monomer volatilization which limits its applications.[59] Thus, it is favorable to reduce the ROP temperature to avoid the partial degradation of the benzoxazine precursors. In the case of the investigated benzoxazine derivatives, the degradation mechanism is different. The degradation of $[_{H,tBu}Bx^{C12,Me}]Cl$, $[_{dtBu}Bx^{C12,Me}]Cl$, and $[_{H,tBu}Bx^{Cy,Me}]Cl$ starts with the elimination of chlorododecane or chlorocyclohexyl as a main product, respectively. Such an elimination seems to initiate ROP and causes the favorable reduction of the temperature of the ROP. Within the presented benzoxazine derivatives, the lowest onset of the exothermic peak of ROP (T_{exo}^{onset}) is exhibited by $[_{H,tBu}Bx^{C12,Me}]Cl$. This benzoxazine has the highest thermal stability, estimated as a temperature of 5 wt % of mass loss ($T_{-5\%}$) (Table 1) and which is directly related to thermal stability, and exhibits the lowest mass loss during heating up to the onset of ROP.

The measured values of the enthalpy of the exothermic effect (ΔH_{exo}) are in the range of the ROP of common benzoxazine monomers, that is, 50−200 J/g.[59] The highest enthalpy ΔH_{exo} is achieved by the monomer $[_{H,tBu}Bx^{Cy,Me}]Cl$ (94.3 J/g), while the exothermic peak of this monomer is narrower. The lower value of ΔH_{exo} of $[_{dtBu}Bx^{Cy,Me}]Cl$ could stem from the sterical hindrance of the *tert*-butyl in the ortho-position of the phenol. The determined values of the heat of polymerization is lower than the actual ones because of the overlapping endothermic effect. There is no exothermic effect on the DSC curve of $[_{dtBu}Bx^{C12,Me}]Cl$.

The common feature of benzoxazine derivatives involves the high temperature limit of the endothermic effect (T_{exo}^{endset}) correlating with the end of the first degradation stage (see Table S3 in Supporting Information).

The experimental results and theoretical calculations provide similar conclusions. The ionic form of benzoxazine presents an N-activated monomer which during curing undergoes transformation into benzoxazine and chloroalkane, after which the mixture forms polymers. Therefore, the mechanism of benzoxazine polymerization by N-activated monomers should be taken into account in theoretical calculations but in a modified fashion that would include the transformation stage presented in this paper.

A detailed description of the polymerization reaction of the *in situ* formed mixture (benzoxazine and chloroalkane) requires in-depth studies on a large set of benzoxazine monomers in order to establish a well-defined structural motif of the obtained polybenzoxazines and the optimization of the polymerization reaction now in progress and will be published with detailed theoretical studies.

3. CONCLUSIONS

A new type of 1,3-benzoxazines have been synthesized by ring-closing reactions of aminophenols activated by NaH. The molecular structure of the newly obtained compounds have been fully characterized in solution by NMR spectroscopy and in the solid state by X-ray. The resulting 1,3-benzoxazine derivatives are well soluble in aqua media, which is crucial inter alia in medical applications. Furthermore, these new compounds can be identified as useful synthons in polymerization reactions, organic synthesis, and in the construction of diverse heterocycles. The most interesting results have been obtained by combined experimental and theoretical studies proving the unique transformation reactions of ionic 1,3-benzoxazine monomers leading to a classical neutral form and chloroalkane, which could be the key stages modifying the commonly proposed mechanism of the ROP process. Generally, both heteroatoms (N, O) on the oxazine ring can be potential cationic polymerization initiation sites, but the oxygen atom is preferred over nitrogen. The alternative route of polymerization is only conceptually possible, also with the nitrogen atom as the initiation site. The current mechanism enforced in the appropriate literature is classical and described extensively, but the intermediate derivatives have not been isolated up to now. The above-presented benzoxazines are examples of such intermediates which illustrate the first stage of monomer initiation occurring on the nitrogen atom. Additionally, the proven alternative route by the chloroalkane formation indicates a new perspective in the discussion on the initiation of monomers.

4. EXPERIMENTAL SECTION

4.1. General Materials, Methods, and Procedures. Solvents for synthesis were purified by standard methods: THF [high-performance liquid chromatography (HPLC), VWR] was distilled from Na/benzophenone, MeOH (HPLC, VWR) was distilled, and DCM (99.8% VWR) was distilled from P_2O_5, *n*-hexane (HPLC, VWR). Solvents for a standard workup and chromatography were used as received. All chemicals were obtained from commercial sources and used without further purification: 2,4-*tert*-buthylphenol (99%, Sigma-Aldrich), 4-*tert*-buthylphenol (99%, Sigma-Aldrich), *N*-methylcyclohexylamine (99%, Sigma-Aldrich) *N*-methyldodecylamine (98%, Alfa Aesar), formaldehyde (37% solution in H_2O, Sigma-Aldrich), and sodium hydride (95%, Sigma-Aldrich).

The ^1H, ^{13}C NMR spectra were obtained using a Bruker AVANCE 500 MHz spectrometer. The chemical shifts are given in ppm relative to the residual signals of the solvent ($CDCl_3$, ^1H: 7.26 ppm, ^{13}C: 77.16 ppm). HRMS spectra were recorded using Bruker MicOTOF-Q spectrometers with Supporting Information ion source and time-of-flight mass analyzer. Microanalyses were conducted with an Elementar CHNS Vario EL III analyzer. All the reactions and operations which required an inert atmosphere of N_2 were performed by using a glovebox (MBraun) or standard Schlenk apparatus and vacuum line techniques.

4.2. Syntheses. Aminophenols were synthesized according to a literature procedure:

2,4-Di-*tert*-butyl-6-((cyclohexyl(methyl)amino)methyl)phenol, $[_{dtBu}L^{Cy,Me}-H]$.[60]

2,4-Di-*tert*-butyl-6-((dodecyl(methyl)amino)methyl)phenol, $[_{dtBu}L^{C12,Me}-H]$.[61]

4-*tert*-Butyl-6-((cyclohexyl(methyl)amino)methyl)phenol, $[_{H,tBu}L^{Cy,Me}-H]$.[62]

4.2.1. 4-tert-Butyl-6-((dodecyl(methyl)amino)methyl)phenol, $_{H,tBu}L^{C12,Me}-H$. To a solution of 0.60 g (4.00 mmol) of 4-*tert*-butylphenol and 1.00 mL (4.00 mmol) of *N*-methyldodecylamine in MeOH (20 mL), 0.45 mL (6.00 mmol) of formaldehyde (37% solution in H_2O) was added. The solution was stirred and heated under reflux for 24 h. Next, the mixture was evaporated to give yellow oil, washed with 20 mL of cold methanol placed in a freezer for recrystallization. The crude product precipitated as a white solid after 1 week. It was collected by filtration, washed with cold methanol (3 × 20 mL), and dried *in vacuo* to give $_{H,tBu}L^{C12,Me}-H$. Yield 72% (1.04 g,

2.88 mmol). ^{1}H NMR (500 MHz, CDCl$_3$): δ 9.54 (s, 1H, OH), 7.17 (dd, J_{HH} = 8.4, 2.4 Hz, 1H, ArCH), 6.94 (d, J_{HH} = 2.4 Hz, 1H, ArCH), 6.75 (d, J_{HH} = 8.4, Hz, 1H, ArCH), 3.67 (s, 2H, ArCH$_2$N), 2.46 (t, J_{HH} = 7.4 Hz, 2H, CH$_2$), 2.27 (s, 3H, NCH$_3$), 1.59−1.48 (m, 2H, CH$_2$), 1.27 (m, 27H, C(CH$_3$)$_3$, CH$_2$), 0.88 (t, J_{HH} = 7.0 Hz, 3H, CH$_3$). ^{13}C NMR (126 MHz, CDCl$_3$): δ 155.72 (s, 1C, ArCO), 141.66 (s, 1C, ArC), 125.37 (s, 1C, ArCH), 125.22 (s, 1C, ArCH), 121.34 (s, 1C, ArC), 115.45 (s, 1C, ArCH), 62.09 (s, 1C, ArCH$_2$N), 57.38 (s, 1C, CH$_2$), 41.34 (s, 1C, NCH$_3$), 34.07 (s, 1C, C(CH$_3$)$_3$), 32.06 (s, 1C, CH$_2$), 31.72 (s, 3C, C(CH$_3$)$_3$), 30.09−29.57 (m, 5C, CH$_2$), 29.49 (s, 1C, CH$_2$), 27.34 (s, 1C, CH$_2$), 27.16 (s, 1C, CH$_2$), 22.83 (s, 1C, CH$_2$), 14.25 (s, 1C, CH$_3$). Anal. calcd (found) for C$_{24}$H$_{43}$NO: C, 79.72 (79.14); H, 11.99 (11.57); N, 3.87 (3.51)%. ESI/MS calcd (found): 361.33 (362.3) [M + 1]$^+$.

4.2.2. 6,8-Di-tert-butyl-3-cyclohexyl-3-methyl-3,4-dihydro-2H-benzo[e][1,3]oxazin-3-yl Chloride, [$_{dtBu}$Bx^{Cy,Me}]Cl. To a solution of $_{dtBu}$L^{Cy,Me}−H (0.50 g, 1.50 mmol) in 10 mL of the mixture of THF/CH$_2$Cl$_2$ (1/1), NaH (0.057 g, 1.89 mmol, 1.25 equiv) was added under a inert atmosphere of N$_2$. The slightly yellow solution was stirred for 1 h until gas evolution disappeared. Then, the mixture was evaporated to dryness and the 15 mL of CH$_2$Cl$_2$ was added for the precipitation of NaCl. After filtration of NaCl, the filtrate was dried over vacuum to give $_{dtBu}$Bx^{Cy,Me} as a white powder (0.51 g, 1.34 mmol) in 89% yield. ^{1}H NMR (500 MHz, CDCl$_3$): δ 7.27 (d, J_{HH} = 2.4 Hz, 1H, ArCH), 6.92 (d, J_{HH} = 2.4 Hz, 1H, ArCH), 5.76 (d, J_{HH} = 8.6 Hz, 1H, NCH$_2$O), 5.56 (d, J_{HH} = 8.6 Hz, 1H, NCH$_2$O), 5.24 (d, J_{HH} = 15.3 Hz, 1H, NCH$_2$Ar), 4.89 (d, J_{HH} = 15.3 Hz, 1H, NCH$_2$Ar), 3.89 (m, 1H, NCH), 3.42 (s, 3H, NCH$_3$), 2.42−2.30 (m, 2H, CH$_2$), 2.08−1.90 (m, 2H, CH$_2$), 1.73−1.62 (m, 1H, CH$_2$), 1.35−1.31 (m, 2H, CH$_2$), 1.34 (s, 9H, C(CH$_3$)$_3$), 1.27 (s, 9H, C(CH$_3$)$_3$), 1.25−1.07 (m, 3H, CH$_2$). ^{13}C NMR (126 MHz, CDCl$_3$): δ 154.92 (s, 1C, ArC-O), 146.64 (s, 1C, ArC), 137.95 (s, 1C, ArC), 124.72 (s, 1C, ArCH), 123.59 (s, 1C, ArCH), 113.64 (s, 1C, ArC), 83.50 (s, 1C, OCH$_2$N), 67.34 (s, 1C, NCH), 58.59 (s, 1C, NCH$_2$Ar), 41.68 (s, 1C, NCH$_3$), 34.99 (s, 1C, C(CH$_3$)$_3$), 34.72 (s, 1C, C(CH$_3$)$_3$), 31.47 (s, 3C, C(CH$_3$)$_3$), 29.75 (s, 3C, C(CH$_3$)$_3$), 26.60−24.95 (m, 5C, CH$_2$). Anal. calcd (found) for C$_{23}$H$_{38}$ClNO: C, 72.64 (72.70); H, 9.89 (10.08); N, 3.51 (3.69)%. IR: 1230, 961 cm^{-1}.

4.2.3. 6-(tert-Butyl)-3-cyclohexyl-3-methyl-3,4-dihydro-2H-benzo[e][1,3]oxazin-3-yl Chloride, $_{H,tBu}$Bx^{Cy,Me}. Synthesis was carried out analogically as for the compound $_{dtBu}$Bx^{Cy,Me} by using appropriate substrates as follows: compound $_{H,tBu}$L^{Cy,Me}−H (0.50 g, 1.80 mmol), NaH (0.054 g, 2.27 mmol, 1.25 equiv). Compound $_{H,tBu}$Bx^{Cy,Me} was obtained as a white powder. Yield: (0.54 g, 1.59 mmol, 88%). ^{1}H NMR (500 MHz, CDCl$_3$): δ 7.28 (dd, J_{HH} = 8.6, 2.3 Hz, 1H, ArCH), 7.07 (d, J_{HH} = 2.3 Hz, 1H, ArCH), 6.91 (d, J_{HH} = 8.6 Hz, 1H, ArCH), 5.70 (d, J_{HH} = 8.6 Hz, 1H, OCH$_2$N), 5.46 (d, J_{HH} = 8.6 Hz, 1H, OCH$_2$N), 5.16 (d, J_{HH} = 15.3 Hz, 1H, NCH$_2$Ar), 4.97 (d, J_{HH} = 15.3 Hz, 1H, NCH$_2$Ar), 3.81 (m, 1H, NCH), 3.38 (s, 3H, NCH$_3$), 2.35−2.23 (m, 2H, CH$_2$), 2.01−1.95 (m, 2H, CH$_2$), 1.72−1.64 (m, 1H, CH$_2$), 1.62−1.54 (m, 2H, CH$_2$), 1.45−1.34 (m, 2H, CH$_2$), 1.26 (s, 9H, C(CH$_3$)$_3$), 1.20−1.04 (m, 1H, CH$_2$). ^{13}C NMR (126 MHz, CDCl$_3$): δ 148.65 (s, 1C, ArC−O), 147.72 (s, 1C, ArC), 127.39 (s, 1C, ArCH), 124.38 (s, 1C, ArCH), 116.77 (s, 1C, ArCH), 114.34 (s, 1C, ArC), 83.84 (s, 1C, OCH$_2$N), 67.38 (s, 1C, NCH), 58.47 (s, 1C, NCH$_2$Ar), 41.69 (s, 1C, NCH$_3$), 34.62 (s, 1C, C(CH$_3$)$_3$), 31.42 (s, 3C, C(CH$_3$)$_3$), 26.48 (s, 1C, CH$_2$), 25.94 (s, 1C, CH$_2$), 25.28 (s, 2C, CH$_2$), 24.88 (s, 1C, CH$_2$). ESI/MS calcd (found): 303.26 (303.22) [M + 1]$^+$. Anal. calcd (found) for C$_{20}$H$_{33}$ClNO: C, 72.98 (73.22); H, 10.75 (10.81); Cl, 8.46 (8.65); N, 3.12 (3.42)%. IR: 1238, 954 cm^{-1}.

4.2.4. 6,8-Di-tert-butyl-3-cyclohexyl-3-methyl-3,4-dihydro-2H-benzo[e][1,3]oxazin-3-yl Chloride, $_{dtBu}$Bx^{C12,Me}. Synthesis was carried out analogically as for the compound $_{dtBu}$Bx^{Cy,Me} by using appropriate substrates as follows: compound $_{dtBu}$L^{C12,Me}−H (0.50 g, 1.20 mmol), NaH (0.036 g, 1.50 mmol, 1.25 equiv). Compound $_{dtBu}$Bx^{C12,Me} was obtained as a white powder. Yield: (0.52 g, 1.11 mmol, 92%). ^{1}H NMR (500 MHz, CDCl$_3$): δ 7.31 (d, J_{HH} = 2.0 Hz, 1H, ArCH), 6.92 (d, J_{HH} = 2.0 Hz, 1H, ArCH), 5.62 (d, J_{HH} = 8.2 Hz, 1H, OCH$_2$N), 5.39 (d, J_{HH} = 8.2 Hz, 1H, OCH$_2$N), 5.11 (d, J_{HH} = 15.3 Hz, 1H, NCH$_2$Ar), 4.88 (d, J_{HH} = 15.3 Hz, 1H, NCH$_2$Ar), 3.80−3.67 (m, 2H,

NCH$_2$), 3.57 (s, 3H, NCH$_3$), 1.89−1.82 (m, 2H, CH$_2$), 1.73−1.69 (m, 2H, CH$_2$), 1.36 (s, 9H, C(CH$_3$)$_3$), 1.29−1.22 (m, 25H, CH$_2$, C(CH$_3$)$_3$), 0.88 (t, J_{HH} = 6.9 Hz, 3H, CH$_3$). ^{13}C NMR (126 MHz, CDCl$_3$): δ 146.90 (s, 1C, ArC-O), 146.18 (s, 1C, ArC), 138.22 (s, 1C, ArC), 124.82 (s, 1C, ArCH), 122.14 (s, 1C, ArCH), 113.40 (s, 1C, ArC), 84.05 (s, 1C, OCH$_2$N), 62.49 (s, 1C NCH$_2$Ar), 60.91 (s, 1C, NCH$_2$), 45.77 (s, 1C, NCH$_3$), 35.01 (s, 1C, C(CH$_3$)$_3$), 34.24 (s, 1C, C(CH$_3$)$_3$), 31.83 (s, 1C, CH$_2$), 31.47 (s, 3C, C(CH$_3$)$_3$), 29.83 (s, 3C, C(CH$_3$)$_3$), 29.78−29.20 (m, 6C, CH$_2$), 26.45 (s, 1C, CH$_2$), 22.80 (s, 1C, CH$_2$), 22.42 (s, 1C, CH$_2$), 14.24 (s, 1C, CH$_3$). Anal. calcd (found) for C$_{29}$H$_{52}$ClNO: C, 74.36 (74.72); H, 11.00 (11.24); Cl, 7.43 (7.60); N, 2.89 (3.00)%. ESI/MS calcd (found): 430.40 (430.37) [M + 1]$^+$. IR: 1230, 962 cm^{-1}.

4.2.5. 6-(tert-Butyl)-3-dodecyl-3-methyl-3,4-dihydro-2H-benzo-[e][1,3]oxazin-3-yl Chloride, $_{H,tBu}$Bx^{C12,Me}. Synthesis was carried out analogically as for the compound $_{dtBu}$Bx^{Cy,Me} by using appropriate substrates as follows: compound $_{H,tBu}$L^{C12,Me}−H (0.50 g, 1.38 mmol), NaH (0.041 g, 1.73 mmol, 1.25 equiv). Compound $_{H,tBu}$Bx^{C12,Me} was obtained as a white powder, yield: (0.49 g, 1.19 mmol, 85%). ^{1}H NMR (500 MHz, CDCl$_3$): δ 7.28 (dd, J_{HH} = 8.6, 2.3 Hz, 1H, ArCH), 7.07 (d, J_{HH} = 2.3 Hz, 1H, ArCH), 6.91 (d, J_{HH} = 8.6 Hz, 1H, ArCH), 5.70 (d, J_{HH} = 8.2 Hz, 1H, OCH$_2$N), 5.46 (d, J_{HH} = 8.2 Hz, 1H, OCH$_2$N), 5.16 (d, J_{HH} = 15.3 Hz, 1H, NCH$_2$Ar), 4.97 (d, J_{HH} = 15.3 Hz, 1H, NCH$_2$Ar), 3.84−3.64 (m, 2H, NCH$_2$), 3.59 (s, 3H, NCH$_3$), 1.94−1.73 (m, 2H, CH$_2$), 1.40−1.30 (m, 2H, CH$_2$), 1.26−1.16 (m, 25H, CH$_2$, C(CH$_3$)$_3$), 0.84 (t, J_{HH} = 6.9 Hz, 3H, CH$_3$). ^{13}C NMR (126 MHz, CDCl$_3$): δ 147.41 (s, 1C, ArC−O), 147.13 (s, 1C, ArC), 127.37 (s, 1C, ArCH), 124.32 (s, 1C, ArCH), 116.78 (s, 1C, ArCH), 113.11 (s, 1C, ArC), 84.37 (s, 1C, OCH$_2$N), 60.42 (s, 1C, NCH$_2$Ar), 59.49 (s, 1C, NCH$_2$), 45.56 (s, 1C, NCH$_3$), 34.52 (s, 1C, C(CH$_3$)$_3$), 31.96 (s, 1C, CH$_2$), 31.39 (s, 3C, C(CH$_3$)$_3$), 30.08−28.49 (m, 6C, CH$_2$), 26.39 (s, 1C, CH$_2$), 22.74 (s, 1C, CH$_2$), 22.34 (s, 1C, CH$_2$), 14.18 (s, 1C, CH$_3$). Anal. calcd (found) for C$_{25}$H$_{44}$ClNO: C, 72.98 (73.22); H, 10.75 (10.81); Cl, 8.46 (8.65); N, 3.12 (3.42)%. ESI/MS calcd (found): 374.34 (374.23) [M + 1]$^+$. IR: 1232, 930 cm^{-1}.

4.3. Thermal Measurement. TGA was performed using TGA/DSC1 Mettler Toledo thermobalance coupled by heated at 230 °C transfer line to a Nicolet iZ10 Thermo Scientific spectrometer. Samples of 10−12 mg were heated with a rate of 10 °C/min from 25 to 1000 °C under 30 mL/min of nitrogen flow. FT-IR gas-phase spectra were collected with a spectral resolution of 4 cm^{-1} with 32 co-added scans.

DSC measurements were performed using the Mettler Toledo DSC1 system, coupled with a Huber TC 100 intracooler. The instrument was calibrated using indium (T_m = 156.6 °C, ΔH_m = 28.45 J/g) and zinc (T_m = 419.7 °C, ΔH_m = 107.00 J/g) standards. Samples (~3.5 mg) were measured in 40 μL aluminum pans under a constant nitrogen purge (60 mL/min) from 0 to 300 °C with heating rate 10° C/min. The TGA and DSC experimental data were processed using the generic STAR^e computer program. For the purpose of data presentation, the DSC, TGA, and FT-IR profiles were exported to OriginPro 64 (v. 9.0) as ASCII files.

4.4. Details of X-Ray Data Analysis. X-ray diffraction data for a suitable crystal of each sample were collected using a Xcalibur CCD Ruby or KUMA KM4 CCD (see Supporting Information, Tables S1 and S2) with a ω scan technique. The data collection and processing utilized CrysAlis suite of programs.[63] The space groups were determined based on systematic absences and intensity statistics. Lorentz polarization corrections were applied. The structures were solved using intrinsic phasing SHELXT-2014/5 and refined by full-matrix least-squares on F^2. All calculations were performed using the SHELX suite of programs.[64] All non-hydrogen atoms were refined with anisotropic displacement parameters. Hydrogen atom positions were calculated with geometry and not allowed to vary. Thermal ellipsoid plots were prepared with 50% of probability displacements for non-hydrogen atoms by using Mercury 3.9 program.[65] All data have been deposited with the Cambridge Crystallographic Data Centre CCDC-2002871 for isomer 1 of [$_{dtBu}$Bx^{Cy,Me}]Cl and -2002871 for isomer 2 of [$_{dtBu}$Bx^{Cy,Me}]Cl. Copies of the data can be obtained

free of charge by application to CCDC, 12 Union Road, Cambridge CB21EZ, UK or e-mail: deposit@ccdc.cam.ac.uk.

4.5. Computational Details. The optimization of the structures have been performed in the gas phase, 0 K using Gaussian16 (C.01), G16, programme.[66] The 6-31+G(d,p) basis and electron density functionals have been used as included in G16. Each structure has been verified by harmonic frequency analysis with no imaginary vibrational frequencies. The geometrical structures of the minima on PES associated with a TS have been verified by the calculation of the IRC paths and subsequent optimization of the structures to the energy minima. The E_a values have been corrected for the vibrational zero-point energy difference (ΔZPVE) with one imaginary frequency projected out.

Topological analysis of electron density and ELF fields has been carried out using the TopMod09 package. The grid step used for the topological analysis was 0.6–0.7 bohr.

ASSOCIATED CONTENT

Ⓢ Supporting Information

The Supporting Information is available free of charge at https://pubs.acs.org/doi/10.1021/acs.macromol.0c02036.

Spectroscopic data (^{1}H, ^{13}C NMR), FT-IR spectra, X-ray data, computational details, and temperature range of the first degradation stage (PDF)

Crystallographic data for isomers 1 and 2 (CIF)

AUTHOR INFORMATION

Corresponding Author

Jolanta Ejfler — *Faculty of Chemistry, University of Wrocław, Wrocław 50-383, Poland;* ⓞ orcid.org/0000-0002-7467-1312; Email: jolanta.ejfler@chem.uni.wroc.pl

Authors

Danuta Trybuła — *Faculty of Chemistry, University of Wrocław, Wrocław 50-383, Poland*

Aleksandra Marszałek-Harych — *Faculty of Chemistry, University of Wrocław, Wrocław 50-383, Poland*

Małgorzata Gazińska — *Department of Engineering and Technology of Polymers, Faculty of Chemistry, Wrocław University of Science and Technology, Wrocław 50-370, Poland*

Sławomir Berski — *Faculty of Chemistry, University of Wrocław, Wrocław 50-383, Poland*

Dawid Jędrzkiewicz — *Faculty of Chemistry, University of Wrocław, Wrocław 50-383, Poland*

Complete contact information is available at:
https://pubs.acs.org/10.1021/acs.macromol.0c02036

Notes

The authors declare no competing financial interest.

ACKNOWLEDGMENTS

REFERENCES

(1) Ishida, H.; Agag, T. *Handbook of Benzoxazine Resins*; Elsevier: Amsterdam, 2011.

(2) Kiskan, B. Adapting Benzoxazine Chemistry for Unconventional Applications. *React. Funct. Polym.* **2018**, *129*, 76–88.

(3) Malakooti, S.; Qin, G.; Mandal, C.; Soni, R.; Taghvaee, T.; Ren, Y.; Chen, H.; Tsao, N.; Shiao, J.; Kulkarni, S. S. Low-Cost, Ambient-Dried, Superhydrophobic, High Strength,Thermally Insulating, and Thermally Resilient Polybenzoxazine Aerogels. *ACS Appl. Polym. Mater.* **2019**, *1*, 2322–2333.

(4) Dai, J.; Yang, S.; Teng, N.; Liu, Y.; Liu, X.; Zhu, J.; Zhao, J. Synthesis of Eugenol-Based Silicon-Containing Benzoxazines and their Applications as Bio-Based Organic Coatings. *Coatings* **2018**, *8*, 88–102.

(5) Ishida, H.; Allen, D. J. Physical and Mechanical Characterization of Near-Zero Shrinkage Polybenzoxazines. *J. Polym. Sci., Part B: Polym. Phys.* **1996**, *34*, 1019–1030.

(6) Dong, J.-P.; Chiu, S.-G.; Hsu, M.-W.; Huang, Y.-J. Effects of Reactive Low-profile Additives on the Volume Shrinkage and Internal Pigmentability for Low-Temperature Cure of Unsaturated Polyester. *J. Appl. Polym. Sci.* **2006**, *100*, 967–979.

(7) Salabert, J.; Sebastián, R. M.; Marquet, J. Photochemical Polymerization of N-Phenyl Mono-1,3-benzoxazines in Aqueous Media. *Macromolecules* **2018**, *51*, 3672–3679.

(8) Sudo, A.; Du, L.-C.; Hirayama, S.; Endo, T. Substituent Effects of N-Alkyl Groups on Thermally Induced Polymerization Behavior of 1,3-Benzoxazines. *J. Polym. Sci., Part A: Polym. Chem.* **2010**, *48*, 2777–2782.

(9) Zhang, K.; Han, L.; Froimowicz, P.; Ishida, H. A Smart Latent Catalyst-Containing Ortho-Trifluoroacetamide Functional Benzoxazine: Precursor for Low Temperature Formation of Very High Performance Polybenzoxazole with Low Dielectric Constant and HighThermal Stability. *Macromolecules* **2017**, *50*, 6552–6560.

(10) Zhang, K.; Yu, X.; Kuo, S.-W. Outstanding Dielectric and Thermal Properties of Main Chain-Type Poly(benzoxazine-co-imide-cosiloxane)-Based Cross-Linked Networks. *Polym. Chem.* **2019**, *10*, 2387–2396.

(11) Liu, J.; Safronava, N.; Lyon, R. E.; Maia, J.; Ishida, H. Enhanced Thermal Property and Flame Retardancy via Intramolecular 5-Membered Ring Hydrogen Bond-Forming Amide Functional Benzoxazine Resins. *Macromolecules* **2018**, *51*, 9982–9991.

(12) Shan, F.; Ohashi, S.; Erlichman, A.; Ishida, H. Non-Flammable Thiazole-Functional Monobenzoxazines: Synthesis, Polymerization, Thermal and Thermomechanical Properties, and Flammability Studies. *Polymer* **2018**, *157*, 38–49.

(13) Liu, C.; Shen, D.; Sebastián, R. M.; Marquet, J.; Schönfeld, R. Mechanistic Studies on Ring-Opening Polymerization of Benzoxazines: A Mechanistically Based Catalyst Design. *Macromolecules* **2011**, *44*, 4616–4622.

(14) Ejfler, J.; Krauzy-Dziedzic, K.; Szafert, S.; Lis, T.; Sobota, P. Novel Chiral and achiral Benzoxazine Monomers and Their Thermal polymerization. *Macromolecules* **2009**, *42*, 4008–4015.

(15) Chutayothin, P.; Ishida, H. Cationic Ring-Opening Polymerization of 1,3-Benzoxazines: Mechanistic Study Using Model Compounds. *Macromolecules* **2010**, *43*, 4562–4572.

(16) Salum, M. L.; Iguchi, D.; Arza, C. R.; Han, L.; Ishida, H.; Froimowicz, P. Making Benzoxazines Greener: Design, Synthesis, and Polymerization of a Biobased Benzoxazine Fulfilling Two Principles of Green Chemistry. *ACS Sustainable Chem. Eng.* **2018**, *6*, 13096–13106.

(17) Dogan, Y. E.; Satilmis, B.; Uyar, T. Synthesis and Characterization of Bio-Based Benzoxazines Derived from Thymol. *J. Appl. Polym. Sci.* **2019**, *136*, 47371.

(18) Arslan, M.; Kiskan, B.; Yagci, Y. Benzoxazine-Based Thermoset with Autonomous Self-Healing and Shape Recovery. *Macromolecules* **2018**, *51*, 10095–10103.

(19) Khan, M.; Halder, K.; Shishatskiy, S.; Filiz, V. Synthesis and Crosslinking of Polyether-Based Main Chain Benzoxazine Polymers and their Gas Separation Performance. *Polymers* **2018**, *10*, 221.

(20) Zhang, S.; Ran, Q.; Fu, Q.; Gu, Y. Preparation of Transparent and Flexible Shape Memory Polybenzoxazine Film Through Chemical Structure Manipulation and Hydrogen Bonding Control. *Macromolecules* **2018**, *51*, 6561–6570.

(21) Arendt-Pindel, A.; Marszałek-Harych, A.; Gębarowska, E.; Gębarowski, T.; Jędrzkiewicz, D.; Pląskowska, E.; Zalewski, D.; Gulia,

N.; Szafert, S.; Ejfler, J. Design and Functionalization of Bioactive Benzoxazines. An Unexpected Ortho-Substitution Effect. *New J. Chem.* **2019**, *43*, 12042−12053.

(22) Lu, G.; Dai, J.; Liu, J.; Tian, S.; Xu, Y.; Teng, N.; Liu, X. A New Sight into Bio-Based Polybenzoxazine: From Tunable Thermal and Mechanical Properties to Excellent Marine Antifouling Performance. *ACS Omega* **2020**, *5*, 3763−3773.

(23) Ge, J.; Wang, F.; Yin, X.; Yu, J.; Ding, B. Polybenzoxazine-Functionalized Melamine Sponges with Enhanced Selective Capillarity for Efficient Oil Spill Cleanup. *ACS Appl. Mater. Interfaces* **2018**, *10*, 40274−40285.

(24) Sawaryn, C.; Landfester, K.; Taden, A. Cationic Polybenzoxazines. A Novel Polyelectrolyte Class with Adjustable Solubility and Unique Hydrogen-Bonding Capabilities. *Macromolecules* **2011**, *44*, 7668−7674.

(25) Mahfud, R.; Agag, T.; Ishida, H.; Shaikh, S.; Qutubuddin, S. Synthesis and evaluation of novel anionic polymeric surfactants based on polybenzoxazines. *Colloid Interface Sci.* **2013**, *407*, 339−347.

(26) Burke, W. J.; Smith, R. P.; Weatherbee, C. N,N-bis-(Hydroxybenzyl)-amines: Synthesis from Phenols, Formaldehyde and Primary Amines. *J. Am. Chem. Soc.* **1952**, *74*, 602−605.

(27) Rivera, A.; Inées Gallo, G.; Elena Gayón, M.; Joseph-Nathan, P. 1,3-bis(2′-Hydroxybenzyl)imidazolidines as Novel Precursors of 3,3′-Ethylene-bis(3,4-dihydro-2H-1,3-benzoxazine). *Synth. Commun.* **1994**, *24*, 2081−2089.

(28) Campl, E. M.; Jackson, W. R.; McCubbin, Q. J.; Trnacek, A. E. Allylic Rearrangements During the Rhodium-Catalysed Reactions of 2-Allyloxybenzylamines and 2-(N-Allyl-N-benzylamino)benzylamine. *J. Chem. Soc., Chem. Commun.* **1994**, *24*, 2763.

(29) Katritzky, A. R.; Xu, Y.-J.; Jain, R. A Novel Dilithiation Approach to 3,4-Dihydro-2H-1,3-benzothiazines, 3,4-Dihydro-2H-1,3-benzoxazines, and 2,3,4,5-Tetrahydro-1,3-benzothiazepines. *J. Org. Chem.* **2002**, *67*, 8234−8236.

(30) Richers, M. T.; Breugst, M.; Platonova, A. Y.; Ullrich, A.; Dieckmann, A.; Houk, K. N.; Seidel, D. Redox Neutral α-Oxygennation of Amines: Reaction Development and Elucidation of the Mechanism. *J. Am. Chem. Soc.* **2014**, *136*, 6123−6135.

(31) Marszałek-Harych, A.; Trybuła, D.; Jędrzkiewicz, D.; Ejfler, J. Scrabbling around in Synthetic Nuances managing Sodium Compounds: Bisphenol/Bisnaphthol Synthesis by Hydroxyl Group Masking. *Inorg. Chem.* **2020**, *59*, 6895−6904.

(32) Gulia, N.; Ejfler, J.; Szafert, S. Macromolecular Polyyne-Containing Benzoxazines for Cross-Linked Polymerization. *Tetrahedron Lett.* **2012**, *53*, 5471−5474.

(33) Becke, A. D. Density-Functional Thermochemistry. III. The Role of Exact Exchange. *J. Chem. Phys.* **1993**, *98*, 5648−5652.

(34) Lee, C.; Yang, W.; Parr, R. G. Development of the Colle-Salvetti Correlation-Energy Formula into a Functional of the Electron Density. *Phys. Rev. B* **1988**, *37*, 785−789.

(35) Vosko, S. H.; Wilk, L.; Nusair, M. Accurate Spin-Dependent Electron Liquid Correlation Energies for Local Spin Density Calculations: a Critical Analysis. *Can. J. Phys.* **1980**, *58*, 1200−1211.

(36) Stephens, P. J.; Devlin, F. J.; Chabalowski, C. F.; Frisch, M. J. Ab Initio Calculation of Vibrational Absorption and Circular Dichroism Spectra Using Density Functional Force Fields. *J. Phys. Chem.* **1994**, *98*, 11623−11627.

(37) Zhao, Y.; Truhlar, D. G. The M06 Suite of Density Functionals for Main Group Thermochemistry, Thermochemical Kinetics, Noncovalent Interactions, Excited States, and Transition Elements: Two New Functionals and Systematic Testing of Four M06-Class Functionals and 12 Other Functionals. *Theor. Chem. Acc.* **2008**, *120*, 215−241.

(38) Adamo, C.; Barone, V. Toward Reliable Density Functional Methods Without Adjustable Parameters: The PBE0 Model. *J. Chem. Phys.* **1999**, *110*, 6158−6170.

(39) Perdew, J. P.; Burke, K.; Wang, Y. Generalized Gradient Approximation for the Exchange − Correlation Hole of a Many − Electron System. *Phys. Rev. B: Condens. Matter Mater. Phys.* **1996**, *54*, 16533−16539.

(40) Ditchfield, R.; Hehre, W. J.; Pople, J. A. Self Consistent Molecular Orbital Methods, IX. An Extended Gaussian Type Basic for Molecular Orbital Studies of Organic Molecules. *J. Chem. Phys.* **1971**, *54*, 724−728.

(41) Clark, T.; Chandrasekhar, J.; Spitznagel, G. W.; Schleyer, P. V. R. Efficient Diffuse Function-Augmented Basis Sets for Anion Calculations. III. The 3-21+G Basis Set for First-Row Elements, Li-F. *J. Comput. Chem.* **1983**, *4*, 294−301.

(42) Hariharan, P. C.; Pople, J. A. The Influence of Polarization Functions on Molecular Orbital Hydrogenation Energies. *Theor. Chim. Acta* **1973**, *28*, 213−222.

(43) Hehre, W. J.; Ditchfield, R.; Pople, J. A. Self-Consistent Molecular Orbital Methods. XII. Further Extensions of Gaussian-Type Basis Sets for Use in Molecular Orbital Studies of Organic Molecules. *J. Chem. Phys.* **1972**, *56*, 2257−2261.

(44) Hohenberg, P.; Kohn, W. Inhomogeneous Electron Gas. *Phys. Rev.* **1964**, *136*, B864−B871.

(45) Kohn, W.; Sham, L. J. Self−Consistent Equations Including Exchange and Correlation Effects. *Phys. Rev.* **1965**, *140*, A1133−A1138.

(46) Parr, R. G.; Yang, W. *Density−Functional Theory of Atoms and Molecules*; Oxford Univ. Press: Oxford, 1989.

(47) Fukui, K. Formulation of the Reaction Coordinate. *J. Phys. Chem.* **1970**, *74*, 4161−4163.

(48) Ishida, K.; Morokuma, K.; Komornicki, A. The Intrinsic Reaction Coordinate. An Ab Initio Calculation for HNC→HCN and $H^-+CH_4→CH_4+H^-$. *J. Chem. Phys.* **1977**, *66*, 2153−2156.

(49) Bader, R. *Atoms in Molecules: A Quantum Theory*; Oxford University Press: USA, 1994, ISBN 978-0-19-855865-1.

(50) Becke, A. D.; Edgecombe, K. E. A Simple Measure of Electron Localization in Atomic and Molecular Systems. *J. Chem. Phys.* **1990**, *92*, 5397−5403.

(51) Silvi, B.; Savin, A. Classification of Chemical Bonds Based on Topological Analysis of Electron Localization Functions. *Nature* **1994**, *371*, 683−686.

(52) Savin, A.; Silvi, B.; Colonna, F. Topological Analysis of the Electron Localization Function Applied to Delocalized Bonds. *Can. J. Chem.* **1996**, *74*, 1088−1096.

(53) Bio-Rad Laboratories, Inc. SpectraBase, http://spectrabase.com 2020.

(54) Coates, J. Interpretation of Infrared Spectra, A Practical Approach, in Encyclopedia of Analytical Chemistry: Applications. *Theory and Instrumentation*; John Wiley & Sons, 2006; pp 1−23.

(55) Dunkers, J.; Ishida, H. Vibrational assignments of 3-alkyl-3, 4-dihydro-6-methyl-2H-1,3-benzoxazines in the Fingerprint Region. *Spectrochim. Acta* **1995**, *51*, 1061−1074.

(56) Agag, T. Preparation and properties of some thermosets derived from allyl-functional naphthoxazines. *J. Appl. Polym. Sci.* **2006**, *100*, 3769−3777.

(57) Uyar, T.; Koyuncu, Z.; Ishida, H.; Hacaloglu, J. Polymerisation and degradation of an aromatic amine-based naphthoxazine. *J. Polym. Degrad. Stab.* **2008**, *93*, 2096−2103.

(58) Sini, N. K.; Endo, T. Toward Elucidating the Role of Number of Oxazine Rings and Intermediates in the Benzoxazine Backbone on their Thermal Characteristics. *Macromolecules* **2016**, *49*, 8466−8478.

(59) Koz, B.; Kiskan, B.; Yagci, Y. A Novel Benzoxazine Monomer with Methacrylate Functionality and its Thermally Curable (Co)-polymers. *Polym. Bull.* **2011**, *66*, 165−174.

(60) Ejfler, J.; Kobyłka, M.; Jerzykiewicz, L. B.; Sobota, P. Highly Efficient Magnesium Initiators for Lactide Polymerization. *Dalton Trans.* **2005**, *11*, 2047−2050.

(61) Jędrzkiewicz, D.; Marszałek-Harych, A.; Ejfler, J. Serendipitous Synthesis Found in the Nuances of Homoleptic Zinc Complex Formation. *Inorg. Chem.* **2018**, *57*, 8169−8180.

(62) Jędrzkiewicz, D.; Ejfler, J.; Gulia, N.; John, Ł.; Szafert, S. Designing Ancillary Ligands for Heteroleptic/Homoleptic Zinc Complex Formation: Synthesis, Structures and Application in ROP of Lactides. *Dalton Trans.* **2015**, *44*, 13700−13715.

(63) *CrysAlisRED Software*; Oxford Diffraction: Wrocław, Poland; pp 1995−2004.

(64) Sheldrick, G. M. A Short History of SHELX. *Acta Crystallogr., Sect. A: Found. Crystallogr.* **2008**, *64*, 112−122.

(65) Macrae, C. F.; Bruno, I. J.; Chisholm, J. A.; Edgington, P. R.; Mccabe, P.; Pidcock, E.; Rodriguez-Monge, L.; Taylor, R.; Van De Streek, J.; Wood, P. A. Mercury CSD 2.0-New Features for the Visualization and Investigation of Crystal Structures. *J. Appl. Cryst.* **2008**, *41*, 466−470.

(66) Frisch, M. J.; Trucks, G. W.; Schlegel, H. B.; Scuseria, G. E.; Robb, M. A.; Cheeseman, J. R.; Scalmani, G.; Barone, V.; Petersson, G. A.; Nakatsuji, H.; Li, X.; Caricato, M.; Marenich, A. V.; Bloino, J.; Janesko, B. G.; Gomperts, R.; Mennucci, B.; Hratchian, H. P.; Ortiz, J. V.; Izmaylov, A. F.; Sonnenberg, J. L.; Williams-Young, D.; Ding, F.; Lipparini, F.; Egidi, F.; Goings, J.; Peng, B.; Petrone, A.; Henderson, T.; Ranasinghe, D.; Zakrzewski, V. G.; Gao, J.; Rega, N.; Zheng, G.; Liang, W.; Hada, M.; Ehara, M.; Toyota, K.; Fukuda, R.; Hasegawa, J.; Ishida, M.; Nakajima, T.; Honda, Y.; Kitao, O.; Nakai, H.; Vreven, T.; Throssell, K.; Montgomery, J. A., Jr.; Peralta, J. E.; Ogliaro, F.; Bearpark, M. J.; Heyd, J. J.; Brothers, E. N.; Kudin, K. N.; Staroverov, V. N.; Keith, T. A.; Kobayashi, R.; Normand, J.; Raghavachari, K.; Rendell, A. P.; Burant, J. C.; Iyengar, S. S.; Tomasi, J.; Cossi, M.; Millam, J. M.; Klene, M.; Adamo, C.; Cammi, R.; Ochterski, J. W.; Martin, R. L.; Morokuma, K.; Farkas, O.; Foresman, J. B.; Fox, D. J. *Gaussian 16*, Revision C.01; Gaussian, Inc.: Wallingford CT, 2016.